Available online at www.sciencedirect.com
SCIENCE DIRECT®
Journal of Sound and Vibration 266 (2003) 49–74
JOURNAL OF SOUND AND VIBRATION
www.elsevier.com/locate/jsvi

Two-dimensional friction oscillator: group-preserving scheme and handy formulae

C.-S. Liu[a,*], H.-K. Hong[b], D.-Y. Liou[c]

[a] *Department of Mechanical and Marine Engineering, National Taiwan Ocean University, Keelung 202-24, Taiwan*
[b] *Department of Civil Engineering, Taiwan University, Taipei, Taiwan*
[c] *Department of System Engineering and Naval Architecture, Taiwan Ocean University, Keelung, Taiwan*

Received 16 January 2001; accepted 2 September 2002

Abstract

With vibration isolation of buildings and turbomachinery blades in mind, we study the dynamic behaviour of a single-mass two-degree-of-freedom oscillator with dry friction damper, viscous damper and elastic spring connected in parallel. The mass is mounted on an elastic supporting plate allowing movement in two directions on a plane. We formulate a multi-dimensional friction model, from which the sliding conditions and the sticking conditions of the mass are derived. For calculations we develop a group-preserving scheme, which preserves the projective proper orthochronous Lorentz group $PSO_o(2,1)$ symmetry of the model in the sliding phase so as to satisfy automatically the sliding conditions at each time step without iteration at all. The oscillator is then subjected to simple harmonic excitations, and the responses are displayed. According to the simple harmonic balance method together with a circular orbit assumption on displacements, we derive closed-form formulae for handily estimating the steady state responses, which are then compared with the results calculated by the group-preserving scheme to confirm the applicability of the formulae. We also derive formulae specifically for a two-dimensional friction oscillator with rigid base support, which include an exact formula of the magnification factor and a simple formula for estimating the minimum driving force amplitude (or the maximum friction force bound) to avoid sticking.

1. Friction oscillator

The study of non-linear hysteretic behaviour of mechanical systems due to friction has been of great interest to engineers and researchers in a variety of engineering fields, since many

*Corresponding author. Tel.: +886-2-2462-2192; fax: +886-2-2462-0836.
E-mail address: csliu@mail.ntou.edu.tw (C.-S. Liu).

0022-460X/03/$ - see front matter © 2003 Elsevier Science Ltd. All rights reserved.
doi:10.1016/S0022-460X(02)01270-1

engineering systems exhibit frictional behaviour under cyclic loading. Fig. 1 shows two vibration isolation cases: (a) using base isolators for buildings [1] and (b) using damper plates for turbomachinery blades [2]. Both utilize the mechanism of contact friction to reduce the vibration amplitude and display non-linear, hysteretic behaviour. A survey of various non-linear friction oscillators was given in, for example, Ref. [1]. More detailed discussions of Coulomb friction can be found in a review article by Ibrahim [2].

In the past the studies of hysteretic systems are most restricted to one-dimensional oscillators; see, for example, Refs. [3,4]. However, a more practical estimation of the effects of external excitations on systems should suitably account for the simultaneous action of the two components of the external excitations. The dry friction dampers used in turbomachinery to reduce the vibration of the turbine blade often exhibit two-dimensional contact friction motion [5,6]. Due to friction character the multi-dimensional problems become much more difficult to analyze than the one-dimensional problems [7–9].

In this paper we consider a two-dimensional friction oscillator subjected to an external force $\mathbf{p}(t)$. The equation of motion of the oscillator can be written as

$$m\ddot{\mathbf{x}}(t) + c\dot{\mathbf{x}}(t) + \mathbf{r}(t) = \mathbf{p}(t), \tag{1}$$

where the boldfaced lower case letters $\mathbf{x}$, $\mathbf{r}$ and $\mathbf{p}$ are the 2×1 matrices of displacement, speed-independent constitutive force, and external force, respectively. The velocity-dependent

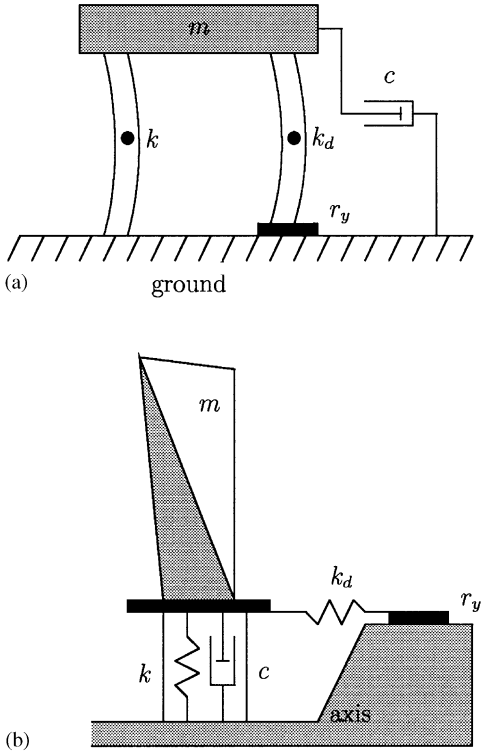

Fig. 1. (a) Building base isolation and (b) vibration abatement of turbomachinery blade which may be simulated by the friction oscillator.

constitutive force $c\dot{\mathbf{x}}$ is due to viscous damping and the speed-independent constitutive force $\mathbf{r}$ is assumed to be the sum of the friction force $\mathbf{r}^a$ and the spring force $\mathbf{r}^b$, i.e.,

$$\mathbf{r} = \mathbf{r}^a + \mathbf{r}^b, \tag{2}$$

with

$$\dot{\mathbf{r}}^b = k\dot{\mathbf{x}}. \tag{3}$$

Eq. (1) together with some prescribed initial conditions $\mathbf{x}(t_i)$ and $\dot{\mathbf{x}}(t_i)$ constitutes an initial-value problem. Here and later t is time and t_i is an initial time; a superposed dot denotes time differentiation; m, c and k are the mass, viscous damping coefficient and elastic spring coefficient, respectively, and $m > 0$, $c \geqslant 0$, $k > 0$ are given.

2. Multi-dimensional friction model

The relation between the friction force $\mathbf{r}^a$ and the displacement $\mathbf{x}$ is assumed to be described by

$$\dot{\mathbf{x}} = \dot{\mathbf{x}}^e + \dot{\mathbf{x}}^f, \tag{4}$$

$$\dot{\mathbf{r}}^a = k_d\dot{\mathbf{x}}^e, \tag{5}$$

$$\dot{\lambda}\mathbf{r}^a = r_y\dot{\mathbf{x}}^f, \tag{6}$$

$$\|\mathbf{r}^a\| \leqslant r_y, \tag{7}$$

$$\dot{\lambda} \geqslant 0, \tag{8}$$

$$\dot{\lambda}\|\mathbf{r}^a\| = r_y\dot{\lambda}, \tag{9}$$

where $k_d > 0$ and $r_y > 0$ are given constants. If the displacement $\mathbf{x}$ is horizontal on the earth ground, the friction force bound r_y is given by $r_y = mg\mu$, where μ is the so-called dynamic coefficient of friction and g is the gravitational acceleration constant. $\|\mathbf{r}^a\|$ is the Euclidean norm of $\mathbf{r}^a$, and $\mathbf{x}^e$ and $\mathbf{x}^f$ are the 2×1 matrices of elastic deformation and frictional slip displacement, respectively, whereas λ is a scalar function of t.

The multi-dimensional friction model (2)–(9) is an extension of the one-dimensional Coulomb friction model [10], which can be realized through a mechanical apparatus as shown in Fig. 2. The model is usually used to simulate the frictional behaviour of base isolators of buildings [1] and damper plates of turbomachinery blades [11–14]; see Fig. 1. An interesting approach to model two-dimensional friction using a discretization procedure has been given in Ref. [15]. The base isolator (or the damper plate) is assumed to be massless, and has the elastic spring coefficient k_d corresponding to the elastic deformation $\mathbf{x}^e$ and the friction force bound r_y corresponding to the frictional slip displacement $\mathbf{x}^f$. It is designed to reduce the vibration of the building (or the blade), which has the mass m, the viscous damping coefficient c, the elastic spring coefficient k, and the displacement $\mathbf{x}$.

The arrangement of mechanical elements schematically drawn in Fig. 3 may help explain the meanings of Eqs. (2)–(9). Eq. (2) decomposes the speed-independent constitutive force $\mathbf{r}$ into the friction force $\mathbf{r}^a$ and the spring force $\mathbf{r}^b$, the latter of which is coaxial with and proportional to $\mathbf{x}$ as

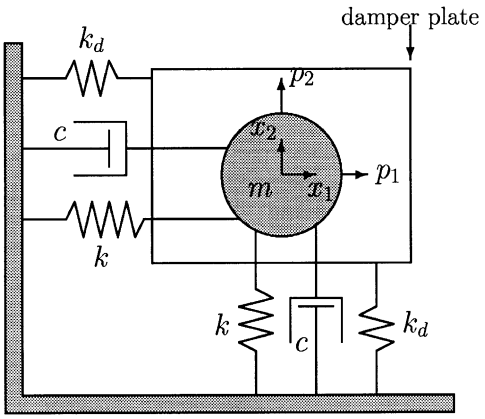

Fig. 2. A mechanical apparatus of the single-mass two-degree-of-freedom friction oscillator.

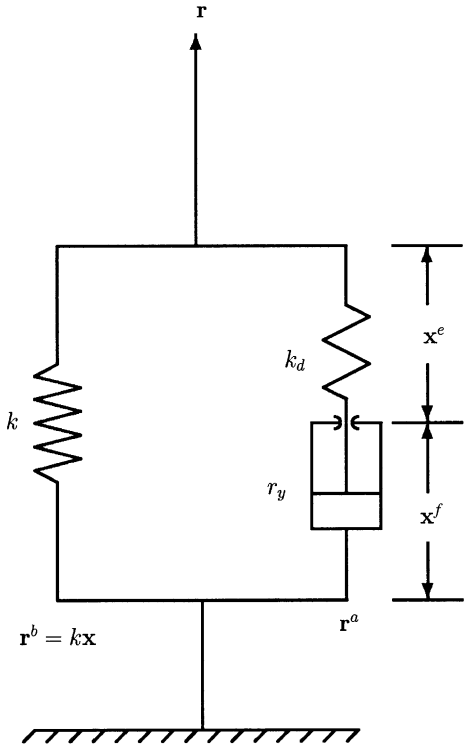

Fig. 3. Schematic drawing showing the connection of mechanical elements.

shown in Eq. (3); Eq. (4) decomposes the displacement $\mathbf{x}$ into the elastic part and the frictional part, the latter of which is the relative slip displacement between the contact surfaces; Eq. (5) expresses the linear law for the elastic part; Eq. (6) is a refined version of the dry friction law relating the friction force $\mathbf{r}^a$ to the frictional slip velocity $\dot{\mathbf{x}}^f$ [10]; inequality (7) specifies the maximum magnitude of the friction force $\mathbf{r}^a$ to be r_y, called the friction force bound; inequality (8)

(with the aid of Eq. (10)) requires the frictional slip speed to be non-negative and hence the arc length of the frictional slip orbit to be never decreasing; and Eq. (9) requires either $\dot{\lambda} = 0$ or $\|\mathbf{r}^a\| = r_y$. This last equation when combined with the two inequalities (7) and (8) is indeed the source of the two phases—the sticking phase and the sliding phase. The significance of the complementary trios (7)–(9) cannot be overemphasized. It furnishes the model with an on–off switch for the mechanism of friction sliding, and the conditions to switch on the mechanism (i.e., the sliding) and the conditions to switch off the mechanism (i.e., the sticking) can thus be derived in a very precise way. Thereby the model can be either in the sliding phase governed by Eqs. (4)–(6) or in the sticking phase governed by $\dot{\mathbf{r}}^a = k_d\dot{\mathbf{x}}$. Further analyses will be given in the following sections.

If we view the frictional slip displacement $\mathbf{x}^f$ as plastic displacement $\mathbf{x}^p$ and r_y as yield strength for an elastoplastic structure, replace Eq. (5) by $\dot{\mathbf{r}} = k_e\dot{\mathbf{x}}^e$, replace Eq. (3) by $\dot{\mathbf{r}}^b = k_p\dot{\mathbf{x}}^p$, and leave the others in Eqs. (1)–(9) unchanged, we have a bilinear oscillator with elastic stiffness k_e and kinematic stiffness k_p. Liu [16] has applied group-preserving scheme to calculate the responses of the bilinear oscillator under harmonic loadings, and has adopted a single-term harmonic balance method to develop closed-form formulae for calculating steady state responses. The present paper applies and extends these methods to the two-dimensional friction oscillator under harmonic loadings. The latter problem has been treated by Griffin and Menq [11], Menq et al. [12,13], and Sanliturk and Ewins [14]. However, these cited papers utilized numerical methods to calculate steady state responses and gave no closed-form formulae for the oscillation amplitude, phase lags, and the minimum force ratio required to prevent the two-dimensional friction oscillator from sticking. The main contributions of the present paper are two-fold: developing a group-preserving scheme to calculate the responses under *general* loading conditions, which guarantees the automatic fulfillment of the sliding conditions without any iteration involved, and deriving closed-form formulae for calculating steady state responses under the assumption of *circular* orbit of displacement. However, Menq and Yang [13] have developed a numerical procedure to calculate steady state responses allowing the orbit of displacement to be *elliptic*.

The present paper does not consider non-planar geometric shapes of the contact damper surfaces such as spherical surfaces, etc., nor the contact force variation and intermittent separation in the direction normal to the contact damper surfaces [17,18]. Nevertheless, if the curved contact surfaces of the friction damper are assumed to be nearly planar, the constitutive relation of the damper can be shown to be equivalent to a parallel combination of an elastic spring (k) and a friction damper (r_y) with planar contact surfaces [19], and hence for such case the method presented herein is still applicable (with $k_d = \infty$). Usually, the three-dimensional contact kinematics and the two-dimensional frictional models also depend on the geometries and types of the friction dampers (or isolators). For these cases and their applications the interested readers are referred to the papers by Yang et al. [18] and Almazán et al. [19].

3. Sliding versus sticking

Taking the Euclidean norm of both sides of Eq. (6) and noting Eqs. (8) and (9) and also $r_y > 0$, we have

$$\dot{\lambda} = \|\dot{\mathbf{x}}^f\|, \tag{10}$$

which tells us that $\lambda(t)$ is nothing but the arc length (mileage) at time t of the frictional slip orbit. By using Eq. (10), Eq. (6) becomes

$$\mathbf{r}^a = r_y \frac{\dot{\mathbf{x}}^f}{\|\dot{\mathbf{x}}^f\|}, \tag{11}$$

if $\|\dot{\mathbf{x}}^f\| > 0$. Note that in the literature, e.g., [11,13], this equation along with inequality (7) was often used to model the multi-dimensional dry friction; however, from the above derivations it is clear that Eqs. (4)–(9) imply Eq. (11), but conversely Eqs. (11) and (7) do not suffice to lead to Eqs. (4)–(9). Especially, when $\|\dot{\mathbf{x}}^f\| = 0$ the above equation is not well defined.

Combining Eqs. (4)–(6), we have

$$\dot{\mathbf{r}}^a + \frac{k_d \dot{\lambda}}{r_y} \mathbf{r}^a = k_d \dot{\mathbf{x}}. \tag{12}$$

The inner product of $\mathbf{r}^a$ with Eq. (12) is

$$k_d \mathbf{r}^a \cdot \dot{\mathbf{x}} = \mathbf{r}^a \cdot \dot{\mathbf{r}}^a + \frac{k_d \dot{\lambda}}{r_y} \mathbf{r}^a \cdot \mathbf{r}^a, \tag{13}$$

which, upon noting the constancy and positivity of both r_y and k_d, asserts that

$$\mathbf{r}^a \cdot \mathbf{r}^a = r_y^2 \Rightarrow \mathbf{r}^a \cdot \dot{\mathbf{x}} = \dot{\lambda} r_y. \tag{14}$$

With this and Eq. (10) we get

$$\dot{\lambda} = \|\dot{\mathbf{x}}^f\| = \frac{1}{r_y} \mathbf{r}^a \cdot \dot{\mathbf{x}} > 0 \quad \text{if } \|\mathbf{r}^a\| = r_y \text{ and } \mathbf{r}^a \cdot \dot{\mathbf{x}} > 0, \tag{15}$$

$$\dot{\lambda} = \|\dot{\mathbf{x}}^f\| = 0 \quad \text{if } \|\mathbf{r}^a\| < r_y \text{ or } \mathbf{r}^a \cdot \dot{\mathbf{x}} \leqslant 0 \text{ or both.} \tag{16}$$

These serve the switching criteria for the mechanism of friction sliding. Thus, Eq. (12) becomes a two-phase non-linear system of equations:

$$\dot{\mathbf{r}}^a = k_d \dot{\mathbf{x}} - \frac{k_d}{r_y^2} \mathbf{r}^a \cdot \dot{\mathbf{x}} \mathbf{r}^a \quad \text{if } \|\mathbf{r}^a\| = r_y \text{ and } \mathbf{r}^a \cdot \dot{\mathbf{x}} > 0, \tag{17}$$

$$\dot{\mathbf{r}}^a = k_d \dot{\mathbf{x}} \quad \text{if } \|\mathbf{r}^a\| < r_y \text{ or } \mathbf{r}^a \cdot \dot{\mathbf{x}} \leqslant 0 \text{ or both.} \tag{18}$$

According to criteria (15) and (16) and the complementary trios (7)–(9), the friction model has two phases (and just two phases): the sliding phase in which $\dot{\lambda} > 0$ and $\|\mathbf{r}^a\| = r_y$, and the sticking phase in which $\dot{\lambda} = 0$ and $\|\mathbf{r}^a\| \leqslant r_y$. In the sliding phase the mechanism of dry friction *sliding* is working so that the contact surfaces slide relative to each other and the model exhibits the energy-dissipative behaviour with the energy dissipation rate $r_y \dot{\lambda} > 0$, which is irreversible, while in the off phase the mechanism of dry friction sliding is shut off and the contact surfaces are *sticking* together so that the model responds elastically and reversibly.

Eqs. (17), (18), (2) and (3) together with the equation of motion (1) constitutes a two-phase third degree non-linear differential equations system for $\mathbf{x}$ and $\mathbf{r}^a$. Usually, the equations are solved by numerical schemes, but it is hard to match the *sliding condition* $\|\mathbf{r}^a\| = r_y$ in the sliding phase unless specifically designed to do so. In the next section, we will design a group-preserving scheme, which fulfills the condition $\|\mathbf{r}^a\| = r_y$ exactly. In Fig. 4(a) the friction force $\mathbf{r}^a$ is

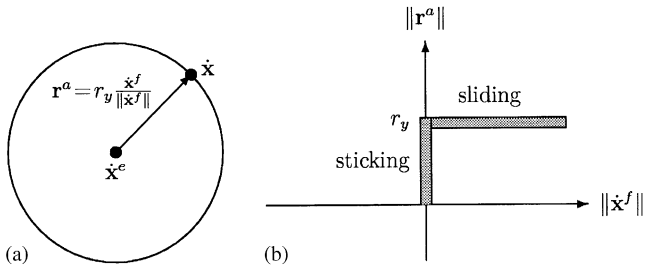

Fig. 4. (a) The allowable friction force region is a disc with radius r_y; the direction of the friction force is $\dot{\mathbf{x}}^f$. (b) Two segments: one segment represents the sliding phase $\{\|\dot{\mathbf{x}}^f\| > 0$ and $\|\mathbf{r}^a\| = r_y\}$ and the other represents the sticking phase $\{\|\dot{\mathbf{x}}^f\| = 0$ and $\|\mathbf{r}^a\| \leqslant r_y\}$.

represented by an oriented vector whose end point is located on the surface $\|\mathbf{r}^a\| = r_y$. In Fig. 4(b) the two-phase characteristic of the model is represented by a two-heavy-segment line.

4. Group-preserving scheme

Define

$$\mathbf{y} := \dot{\mathbf{x}}.$$

Then it follows from Eqs. (1)–(3) and (17) that

$$\dot{\mathbf{x}} = \mathbf{y}, \tag{19}$$

$$\dot{\mathbf{y}} = -\frac{1}{m}(k\mathbf{x} + c\mathbf{y} + \mathbf{r}^a - \mathbf{p}), \tag{20}$$

$$\dot{\mathbf{r}}^a = k_d\mathbf{y} - \frac{k_d}{r_y^2}\mathbf{r}^a \cdot \mathbf{y}\mathbf{r}^a. \tag{21}$$

They are cubic non-linear differential equations system in space $(\mathbf{x}, \mathbf{y}, \mathbf{r}^a)$, governing the motion in the sliding phase. In the sticking phase the equations are rather simple as follows:

$$\dot{\mathbf{x}} = \mathbf{y}, \tag{22}$$

$$\dot{\mathbf{y}} = -\frac{k + k_d}{m}\mathbf{x} - \frac{c}{m}\mathbf{y} + \frac{1}{m}\mathbf{p}. \tag{23}$$

From Eqs. (19)–(21) it is obvious that the source of the non-linearity of the model system is the constitutive relation of $\mathbf{r}^a$ and $\mathbf{y}$. In order to enhance the computational accuracy and efficiency, let us return to Eqs. (12) and (15) in the sliding phase. Upon introducing the integrating factor

$$X^0 := \exp\left(\frac{k_d\lambda}{r_y}\right), \tag{24}$$

and by using Eqs. (15), (19) and (21), we have

$$\frac{\mathrm{d}}{\mathrm{d}t}\begin{bmatrix} X^0\mathbf{r}^a/r_y \\ X^0 \end{bmatrix} = \mathbf{A}\begin{bmatrix} X^0\mathbf{r}^a/r_y \\ X^0 \end{bmatrix}, \tag{25}$$

where

$$\mathbf{A} := \frac{k_d}{r_y}\begin{bmatrix} 0 & 0 & y_1 \\ 0 & 0 & y_2 \\ y_1 & y_2 & 0 \end{bmatrix} \tag{26}$$

satisfies

$$\mathbf{A}^{\mathrm{t}}\mathbf{g} + \mathbf{g}\mathbf{A} = \mathbf{0}, \tag{27}$$

with

$$\mathbf{g} := \begin{bmatrix} 1 & 0 & 0 \\ 0 & 1 & 0 \\ 0 & 0 & -1 \end{bmatrix} \tag{28}$$

the metric of the Minkowski space $\mathbb{M}^3$. In above the superscript t denotes the transpose. The group $\{\mathbf{G}\}$ generated from the algebra $\{\mathbf{A}\}$ is an element of the proper orthochronous Lorentz group $SO_o(2,1)$, preserving the metric $\mathbf{g}$,

$$\mathbf{G}^{\mathrm{t}}\mathbf{g}\mathbf{G} = \mathbf{g}. \tag{29}$$

Accordingly, a group-preserving scheme [20] of the time-centered Euler type is available for Eq. (25),

$$\begin{bmatrix} X^0(n+1)\mathbf{r}^a(n+1)/r_y \\ X^0(n+1) \end{bmatrix} = [\mathbf{I} - \tau\mathbf{A}(n)]^{-1}[\mathbf{I} + \tau\mathbf{A}(n)]\begin{bmatrix} X^0(n)\mathbf{r}^a(n)/r_y \\ X^0(n) \end{bmatrix}, \tag{30}$$

where $\mathbf{r}^a(n)$ denotes the numerical value of $\mathbf{r}^a$ at a discrete time t_n and so on, and τ is one half of the time increment, that is, $\tau := \Delta t/2 = (t_{n+1} - t_n)/2$. Substituting Eq. (26) for $\mathbf{A}$ in the above equation and taking projection yields

$$r_1^a(n+1) = \frac{(\tau^2 k_d^2[y_1^2(n) - y_2^2(n)] + r_y^2)r_1^a(n) + 2\tau^2 k_d^2 y_1(n)y_2(n)r_2^a(n) + 2\tau k_d r_y^2 y_1(n)}{2\tau k_d y_1(n)r_1^a(n) + 2\tau k_d y_2(n)r_2^a(n) + \tau^2 k_d^2[y_1^2(n) + y_2^2(n)] + r_y^2}, \tag{31}$$

$$r_2^a(n+1) = \frac{(\tau^2 k_d^2[y_2^2(n) - y_1^2(n)] + r_y^2)r_2^a(n) + 2\tau^2 k_d^2 y_1(n)y_2(n)r_1^a(n) + 2\tau k_d r_y^2 y_2(n)}{2\tau k_d y_1(n)r_1^a(n) + 2\tau k_d y_2(n)r_2^a(n) + \tau^2 k_d^2[y_1^2(n) + y_2^2(n)] + r_y^2}. \tag{32}$$

Eqs. (31) and (32) together with the discretizations of Eqs. (19) and (20) constitute a numerical scheme for the non-linear system in the sliding phase,

$$x_1(n+1) = x_1(n) + \Delta t y_1(n), \tag{33}$$

$$x_2(n+1) = x_2(n) + \Delta t y_2(n), \tag{34}$$

$$y_1(n+1) = y_1(n) - \frac{1}{m}\Delta t[kx_1(n) + cy_1(n) + r_1^a(n) - p_1(n)], \tag{35}$$

$$y_2(n+1) = y_2(n) - \frac{1}{m}\Delta t[kx_2(n) + cy_2(n) + r_2^a(n) - p_2(n)]. \tag{36}$$

From Eqs. (31) and (32) it follows that

$$\|\mathbf{r}^a(n)\| = r_y \Rightarrow \|\mathbf{r}^a(n+1)\| = r_y$$

for each time increment in the sliding phase; therefore, this scheme is remarkably guaranteed to match exactly the sliding condition $\|\mathbf{r}^a\| = r_y$. So we emphasize that the group-preserving scheme as shown by Eqs. (31)–(36) is much more accurate, efficient and stable than conventional numerical schemes, because the new scheme preserves the internal symmetry $PSO_o(2,1)$, the projective proper orthochronous Lorentz group, of the model in the sliding phase so as to satisfy automatically the sliding conditions at each time step without iteration at all.

5. Numerical results

In the remainder of the paper let us restrict the two-dimensional external force $\mathbf{p}(t)$ to be simple harmonic,

$$p_1(t) = p_0 \cos \omega_d t, \tag{37}$$

$$p_2(t) = p_0 \sin \omega_d t, \tag{38}$$

with amplitude p_0 and driving circular frequency ω_d.

Under the above excitation the oscillator in the sticking phase is governed by

$$m\ddot{x}_1(t) + c\dot{x}_1(t) + (k + k_d)x_1(t) = p_0 \cos \omega_d t + k_d x_1(t_i) - r_1^a(t_i), \tag{39}$$

$$m\ddot{x}_2(t) + c\dot{x}_2(t) + (k + k_d)x_2(t) = p_0 \sin \omega_d t + k_d x_2(t_i) - r_2^a(t_i), \tag{40}$$

where t_i is the initial time of the sticking phase. Let

$$\delta := \frac{4(k + k_d)}{m} - \frac{c^2}{m^2} > 0, \qquad a := \frac{-c}{2m}, \qquad b := \frac{\sqrt{\delta}}{2}. \tag{41–43}$$

Eqs. (39) and (40) have the following closed-form solutions:

$$
\begin{aligned}
x_1(t) = {} & x_1(t_i) + \frac{e^{a(t-t_i)}}{b}\sin b(t-t_i)\dot{x}_1(t_i) \\
& - \left\{\frac{e^{a(t-t_i)}}{bm(a^2+b^2)}[a\sin b(t-t_i) - b\cos b(t-t_i)] + \frac{1}{m(a^2+b^2)}\right\}[r_1^a(t_i) + kx_1(t_i)] \\
& + \frac{p_0}{bm}\frac{(b-\omega_d)\cos\omega_d t - a\sin\omega_d t}{2[a^2+(\omega_d-b)^2]} + \frac{p_0}{bm}\frac{(\omega_d+b)\cos\omega_d t + a\sin\omega_d t}{2[a^2+(\omega_d+b)^2]} \\
& + \frac{p_0 e^{a(t-t_i)}}{bm}\frac{(\omega_d-b)\cos[b(t-t_i)+\omega_d t_i] + a\sin[b(t-t_i)+\omega_d t_i]}{2[a^2+(\omega_d-b)^2]} \\
& + \frac{p_0 e^{a(t-t_i)}}{bm}\frac{a\sin[b(t-t_i)-\omega_d t_i] - (\omega_d+b)\cos[b(t-t_i)-\omega_d t_i]}{2[a^2+(\omega_d+b)^2]},
\end{aligned}
\tag{44}
$$

$$
\begin{aligned}
x_2(t) = {} & x_2(t_i) + \frac{e^{a(t-t_i)}}{b}\sin b(t-t_i)\dot{x}_2(t_i) \\
& - \left\{\frac{e^{a(t-t_i)}}{bm(a^2+b^2)}[a\sin b(t-t_i) - b\cos b(t-t_i)] + \frac{1}{m(a^2+b^2)}\right\}[r_2^a(t_i) + kx_2(t_i)] \\
& + \frac{p_0}{bm}\frac{a\cos\omega_d t + (b-\omega_d)\sin\omega_d t}{2[a^2+(\omega_d-b)^2]} + \frac{p_0}{bm}\frac{(\omega_d+b)\sin\omega_d t - a\cos\omega_d t}{2[a^2+(\omega_d+b)^2]} \\
& + \frac{p_0 e^{a(t-t_i)}}{bm}\frac{(\omega_d-b)\sin[b(t-t_i)+\omega_d t_i] - a\cos[b(t-t_i)+\omega_d t_i]}{2[a^2+(\omega_d-b)^2]} \\
& + \frac{p_0 e^{a(t-t_i)}}{bm}\frac{(\omega_d+b)\sin[b(t-t_i)-\omega_d t_i] + a\cos[b(t-t_i)-\omega_d t_i]}{2[a^2+(\omega_d+b)^2]}.
\end{aligned}
\tag{45}
$$

In the sliding phase the governing equations are however highly non-linear, so we use schemes (31)–(36) to calculate the responses. For the purposes of demonstration we give two typical cases. The first one adopted the following parameters: $m = 2500/\pi^2$ kN s^2/m ($= 2.5\times10^6/(9.81\pi^2)$ kg), $c = 200/\pi$ kN s/m, $k_d = 50\,000$ kN/m, $k = 10\,000$ kN/m, $r_y = 50$ kN, $p_0 = 250$ kN, and $\omega_d = 20\pi$ rad/s. For the non-steady state the behaviour is rather complicated, because the transition from one phase to another phase may occur consecutively as shown in Fig. 5(h). The responses are displayed in Figs. 5(a)–(h). The other case adopted the following parameters: $m = 22\,500/\pi^2$ kN s^2/m ($= 2.25\times10^7/(9.81\pi^2)$ kg), $c = 600/\pi$ kN s/m, $k_d = 50\,000$ kN/m, $k = 10\,000$ kN/m, $r_y = 50$ kN, $p_0 = 500$ kN, and $\omega_d = 4\pi$ rad/s. The transition from the sticking phase to the sliding phase occurred at the moment when the friction force reached the sliding circle as shown in Fig. 6(h), and after two such transitions it remained to be in the sliding phase. The scheme as can be seen preserves exactly one of the sliding conditions, $\|\mathbf{r}^a\| = r_y$, during the sliding phase. The responses are displayed in Figs. 6(a)–(h), which are observed to tend to the steady state. So in the following two sections we seek the steady state, constant amplitude solutions to the responses via a simple first order harmonic balance method.

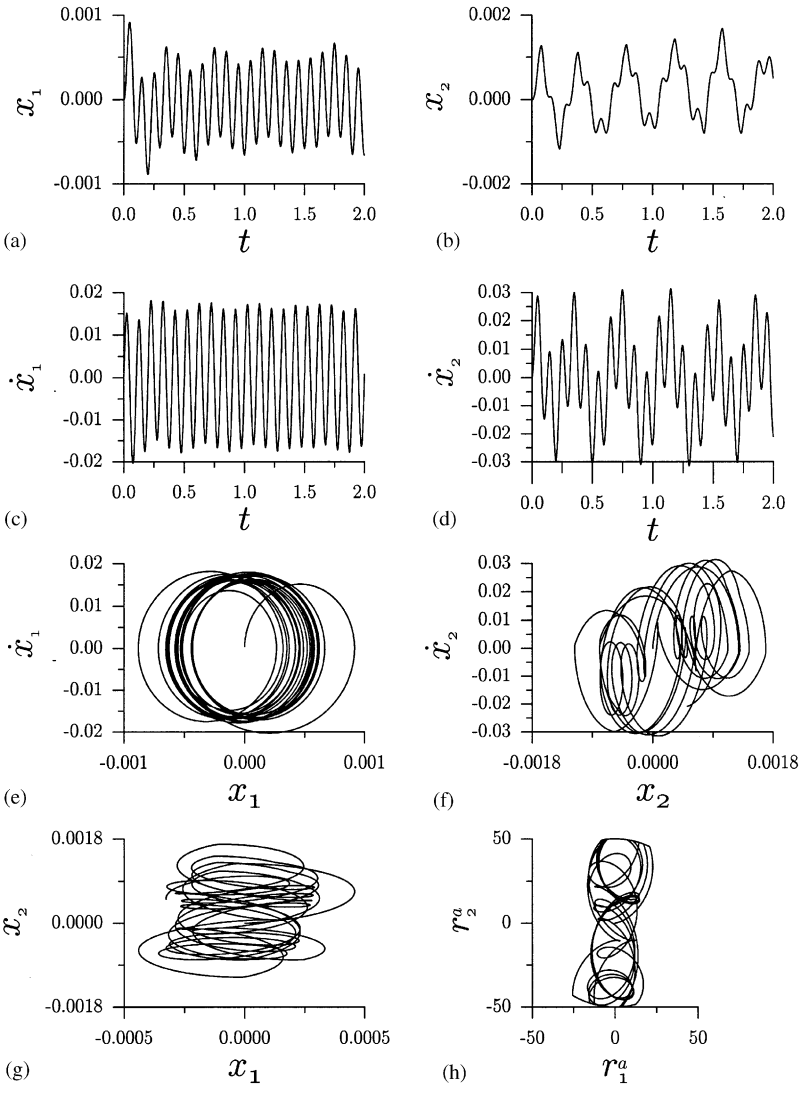

Fig. 5. A typical response of the friction oscillator under small driving force showing non-steady state behaviour. Time histories of displacements: (a) x_1 and (b) x_2, and of velocities (c) $\dot{x}_1$ and (d) $\dot{x}_2$; phase trajectories of $(x_1, \dot{x}_1)$ in (e) and of $(x_2, \dot{x}_2)$ in (f); and response paths of (x_1, x_2) in (g) and of (r_1^a, r_2^a) in (h).

6. Steady state responses of circular type

A closed-form estimation of the steady state responses of the one-dimensional Coulomb friction oscillator under harmonic loadings has been obtained in Ref. [21]. Here, we extend those results to the two-dimensional friction oscillator. Some related issues have been discussed by Griffin and Menq [11], Menq et al. [12,13], and Sanliturk and Ewins [14]. However, these papers gave no closed-form formulae for the oscillation amplitude or the minimum force ratio required to prevent the two-dimensional friction oscillator from sticking.

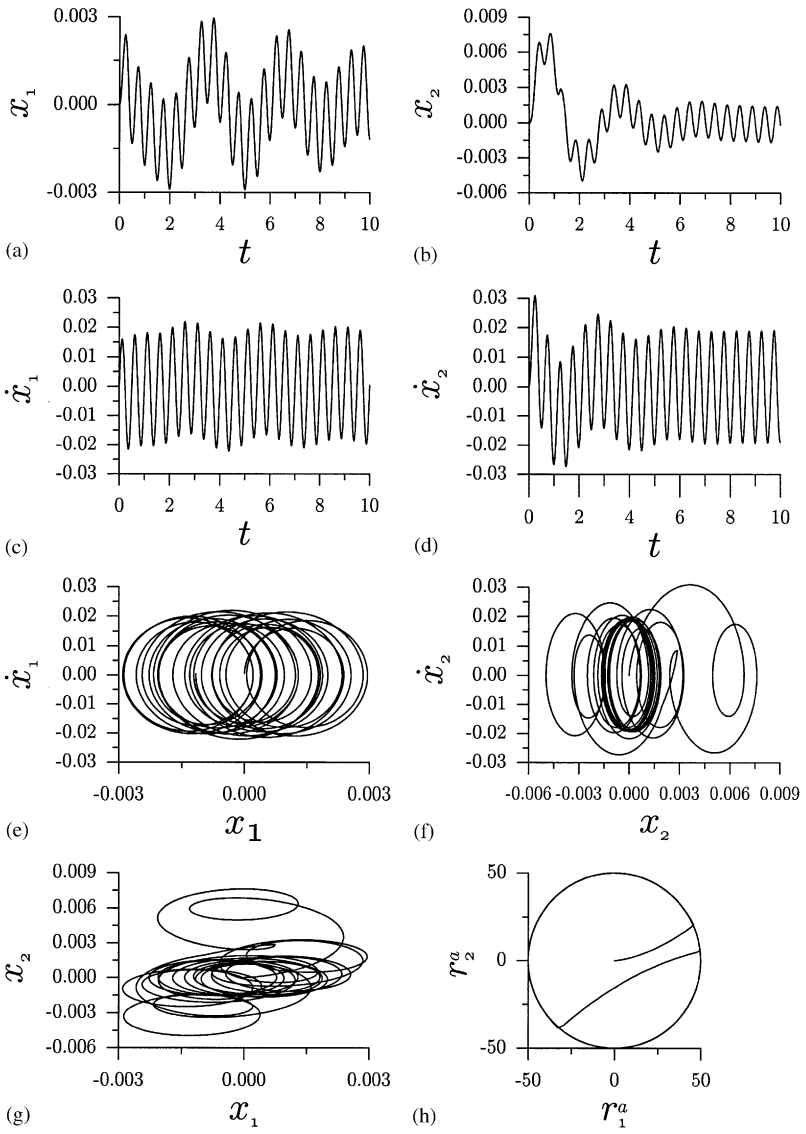

Fig. 6. A typical response of the friction oscillator under large driving force which shows steady state behaviour. Time histories of displacements: (a) x_1 and (b) x_2, and of velocities (c) $\dot{x}_1$ and (d) $\dot{x}_2$; phase trajectories of $(x_1, \dot{x}_1)$ in (e) and of $(x_2, \dot{x}_2)$ in (f); response paths of (x_1, x_2) in (g) and of (r_1^a, r_2^a) in (h).

Let us consider steady state sliding oscillation, and assume that the friction forces are described by

$$r_1^a = r_y \cos\theta, \tag{46}$$

$$r_2^a = r_y \sin\theta, \tag{47}$$

which leave an unknown phase θ to be determined. By Eq. (17) it follows that

$$\dot{\theta} = \frac{k_d}{r_y}[\dot{x}_2 \cos\theta - \dot{x}_1 \sin\theta], \tag{48}$$

and, at the same time, Eq. (15) reduces to

$$\dot{\lambda} = \dot{x}_1 \cos\theta + \dot{x}_2 \sin\theta. \tag{49}$$

Furthermore, the displacements in the steady state are assumed to be located on a circle with radius x_0 and have the following forms:

$$x_1 = x_0 \cos\theta_1, \tag{50}$$

$$x_2 = x_0 \sin\theta_1, \tag{51}$$

whose phase

$$\theta_1 := \omega_d t - \phi \tag{52}$$

has a phase lag ϕ with the phase of the external excitations. We also let the phase of the friction forces has a phase lag ψ with the phase of the displacements, i.e.,

$$\theta := \theta_1 - \psi. \tag{53}$$

Three unknowns x_0, ϕ and ψ are involved in the above formulations, so we need three equations to solve them. These equations will be derived below.

Substituting Eqs. (50) and (51) into Eq. (49) and using Eq. (53), render

$$\dot{\lambda} = -x_0 \omega_d \sin\psi. \tag{54}$$

Utilizing this $\dot{\lambda}$ in Eq. (12) we have

$$\dot{r}_1^a = k_d \dot{x}_1 + \frac{k_d x_0 \omega_d \sin\psi}{r_y} r_1^a, \tag{55}$$

$$\dot{r}_2^a = k_d \dot{x}_2 + \frac{k_d x_0 \omega_d \sin\psi}{r_y} r_2^a. \tag{56}$$

Substituting Eqs. (46), (47), (50) and (51) into the above two equations and using $\dot{\theta} = \omega_d$ give, respectively,

$$-r_y \sin\theta = -k_d x_0 \sin\theta_1 + k_d x_0 \sin\psi \cos\theta, \tag{57}$$

$$r_y \cos\theta = k_d x_0 \cos\theta_1 + k_d x_0 \sin\psi \sin\theta, \tag{58}$$

which, upon taking account of Eq. (53), lead to

$$-r_y \sin\theta = -k_d x_0 \sin\theta \cos\psi, \tag{59}$$

$$r_y \cos\theta = k_d x_0 \cos\theta \cos\psi. \tag{60}$$

Both the above two equations result in

$$r_y = k_d x_0 \cos\psi. \tag{61}$$

Similarly, substituting Eqs. (46), (47), (50), (51), (37) and (38) into Eq. (1) we have

$$-m\omega_d^2 x_0 \cos\theta_1 = c\omega_d x_0 \sin\theta_1 - kx_0 \cos\theta_1 - r_y \cos\theta + p_0 \cos\omega_d t, \tag{62}$$

$$m\omega_d^2 x_0 \sin\theta_1 = c\omega_d x_0 \cos\theta_1 + kx_0 \sin\theta_1 + r_y \sin\theta - p_0 \sin\omega_d t. \tag{63}$$

The second equation is not independent of the first one, because it is the time derivative of the first equation. Now using Eqs. (52) and (53) we obtain

$$-m\omega_d^2 x_0 \cos\theta_1 = c\omega_d x_0 \sin\theta_1 - kx_0 \cos\theta_1 - r_y \cos(\theta_1 - \psi) + p_0 \cos(\theta_1 + \phi), \tag{64}$$

which requires the coefficients before $\cos\theta_1$ and $\sin\theta_1$, respectively, to vanish, as shown below

$$(m\omega_d^2 - k)x_0 - r_y \cos\psi + p_0 \cos\phi = 0, \tag{65}$$

$$c\omega_d x_0 - r_y \sin\psi - p_0 \sin\phi = 0. \tag{66}$$

See also the derivations made by Griffin and Menq [11], and Eqs. (23) and (24) appeared therein. However, Griffin and Menq obtained the following equation:

$$\left[(k - m\omega_d^2)x_0 + \frac{r_y^2}{k_d x_0}\right]^2 + \left[c\omega_d x_0 + r_y\sqrt{1 - \left(\frac{r_y}{k_d x_0}\right)^2}\right]^2 = p_0^2$$

by squaring Eqs. (65) and (66), adding them together, and substituting the result from Eq. (61) for $\cos\psi$ and $-[1 - r_y^2/(k_d x_0)^2]^{1/2}$ for $\sin\psi$, but they did not succeed in solving it for x_0, and appealed its solution to a numerical method.

To proceed we solve Eqs. (65) and (66) in closed form. Divided by r_y they may be non-dimensionalized as follows:

$$r_k(r_w^2 - 1)\hat{x}_0 - \cos\psi + r_f \cos\phi = 0, \tag{67}$$

$$2\zeta r_k r_w \hat{x}_0 - \sin\psi - r_f \sin\phi = 0, \tag{68}$$

where

$$\hat{x}_0 := \frac{k_d x_0}{r_y} \tag{69}$$

is called the magnification factor, and

$$r_f := \frac{p_0}{r_y}, \tag{70}$$

$$r_k := \frac{k}{k_d}, \tag{71}$$

$$r_w := \frac{\omega_d}{\omega_n}, \tag{72}$$

$$\zeta := \frac{c}{2\sqrt{mk}} \tag{73}$$

are dimensionless ratios: r_f is the ratio of the amplitude of the driving force to the friction force bound; r_k is the ratio of the stiffnesses of damper mass and damper plate; r_w is the ratio of the

driving frequency to the natural frequency of the damper mass, $\omega_n := \sqrt{k/m}$; and ζ is the damping ratio.

From Eqs. (61) and (69) it follows that $\cos\psi = 1/\hat{x}_0$, and that

$$\sin\psi = -\sqrt{1 - \frac{1}{\hat{x}_0^2}}. \tag{74}$$

The rationale for taking a minus sign before the square root is $-\sin\psi > 0$ via Eqs. (54) and (8). Substituting Eqs. (67) and (68) for $r_f\cos\phi$ and for $r_f\sin\phi$, respectively, into the identity $(r_f\cos\phi)^2 + (r_f\sin\phi)^2 = r_f^2$, and using $1/\hat{x}_0$ for $\cos\psi$ and Eq. (74) for $\sin\psi$, we obtain a single equation for $\hat{x}_0$,

$$\hat{a}_1 - \hat{a}_2\hat{x}_0^2 = \hat{a}_3\sqrt{\hat{x}_0^2 - 1}, \tag{75}$$

where

$$\hat{a}_1 := r_f^2 + 2r_k(r_w^2 - 1) - 1, \tag{76}$$

$$\hat{a}_2 := r_k^2[4\zeta^2 r_w^2 + (r_w^2 - 1)^2], \tag{77}$$

$$\hat{a}_3 := 4\zeta r_k r_w. \tag{78}$$

Squaring both the sides of Eq. (75), we obtain

$$\hat{a}_2^2\hat{x}_0^4 - (2\hat{a}_1\hat{a}_2 + \hat{a}_3^2)\hat{x}_0^2 + \hat{a}_1^2 + \hat{a}_3^2 = 0. \tag{79}$$

Solving this equation for $\hat{x}_0$ we obtain two roots as follows:

$$\hat{x}_0 = \sqrt{\frac{2\hat{a}_1\hat{a}_2 + \hat{a}_3^2 \pm \hat{a}_3\sqrt{4\hat{a}_1\hat{a}_2 + \hat{a}_3^2 - 4\hat{a}_2^2}}{2\hat{a}_2^2}}, \tag{80}$$

while the two phase lags ψ and ϕ can be expressed, respectively, as

$$\psi = -arccos\frac{1}{\hat{x}_0}, \tag{81}$$

$$\phi = arctan\frac{2\zeta r_k r_w\hat{x}_0^2 + \sqrt{\hat{x}_0^2 - 1}}{1 - r_k\hat{x}_0^2(r_w^2 - 1)}. \tag{82}$$

The first equation follows from $\cos\psi = 1/\hat{x}_0$ straightforward; however, the reason for taking a minus sign before arccos is for $-\sin\psi > 0$ as just mentioned, such that $\psi \in [-\pi/2, 0)$ and that $\dot{\lambda} > 0$ in the steady state sliding phase. The second equation is obtained by dividing Eq. (68) by Eq. (67), and substituting $1/\hat{x}_0$ for $\cos\psi$ and Eq. (74) for $\sin\psi$.

Here we have succeeded in transforming the dependence of the steady state responses on the seven parameters, m, c, k, k_d, r_y, p_0, ω_d, to on the four dimensionless parameters, r_f, r_k, r_w, ζ. This achievement may greatly reduce our work in analyzing the steady state behaviour, and gives us a more complete information about the steady state behaviour for different values of the parameters.

For Eq. (80) we should consider two cases, namely

(i) $4\hat{a}_1\hat{a}_2 + \hat{a}_3^2 - 4\hat{a}_2^2 < 0$ non-steady state,
(ii) $4\hat{a}_1\hat{a}_2 + \hat{a}_3^2 - 4\hat{a}_2^2 \geqslant 0$ steady state.

For the latter case it is obvious that

$$\left[\sqrt{4\hat{a}_1\hat{a}_2 + \hat{a}_3^2 - 4\hat{a}_2^2} - \hat{a}_3\right]^2 \geqslant 0, \tag{83}$$

which is equivalent to

$$2\hat{a}_1\hat{a}_2 + \hat{a}_3^2 - \hat{a}_3\sqrt{4\hat{a}_1\hat{a}_2 + \hat{a}_3^2 - 4\hat{a}_2^2} \geqslant 2\hat{a}_2^2 \geqslant 0. \tag{84}$$

From Eqs. (80) and (84) it follows that

$$\hat{x}_0 \geqslant 1, \tag{85}$$

which asserts that the magnification factor for the steady state case is never less than one. We below consider only the steady state case.

Now, we prove that the exact solution of $\hat{x}_0$ in Eq. (80) only takes values in the lower branch curve, that is,

$$\hat{x}_0 = \sqrt{\frac{2\hat{a}_1\hat{a}_2 + \hat{a}_3^2 - \hat{a}_3\sqrt{4\hat{a}_1\hat{a}_2 + \hat{a}_3^2 - 4\hat{a}_2^2}}{2\hat{a}_2^2}}. \tag{86}$$

If it is not so we take the square to obtain

$$\hat{x}_0^2 = \frac{2\hat{a}_1\hat{a}_2 + \hat{a}_3^2 + \hat{a}_3\sqrt{4\hat{a}_1\hat{a}_2 + \hat{a}_3^2 - 4\hat{a}_2^2}}{2\hat{a}_2^2},$$

and substitute it into Eq. (75) for $\hat{x}_0^2$ on the left-hand side, giving

$$\frac{-\hat{a}_3^2 - \hat{a}_3\sqrt{4\hat{a}_1\hat{a}_2 + \hat{a}_3^2 - 4\hat{a}_2^2}}{2\hat{a}_2^2} = \hat{a}_3\sqrt{\hat{x}_0^2 - 1}.$$

Because $\hat{a}_3$ is positive and $\hat{x}_0 \geqslant 1$ under the condition $4\hat{a}_1\hat{a}_2 + \hat{a}_3^2 - 4\hat{a}_2^2 \geqslant 0$ as just proved, the right-hand side is non-negative, but the left-hand side is obviously negative, leading to a contradiction. Hence formula (86) has been proved.

Menq and Yang [13] studied the same problem by using the single-term harmonic balance scheme together with the non-linear differential equations of motion, which were then converted to a set of non-linear algebraic equations in terms of the unknown motion's amplitude and phase. These non-linear algebraic equations as Menq and Yang ([13, Subsection 5.2]) said were then solved iteratively to yield solutions. However, we have exactly derived formula (86) for the motion's amplitude, formula (82) for its phase lag with respect to the external excitation, and formula (81) for the phase lag of the friction force with respect to the displacement.

7. The minimum force ratio to avoid sticking

Through the above discussion we know that the bifurcation equation is

$$4\hat{a}_1\hat{a}_2 + \hat{a}_3^2 - 4\hat{a}_2^2 = 0, \tag{87}$$

which is a polynomial equation of r_f, r_k, r_w and ζ, and is the boundary between two distinct types of long-term behaviour, steady state and non-steady state. The above equation with the aid of definitions (76)–(78) can be written as

$$r_f = \sqrt{1 + 2r_k(1 - r_w^2) + \frac{r_k^2[4\zeta^2 r_w^2 + (r_w^2 - 1)^2]^2 - 4\zeta^2 r_w^2}{4\zeta^2 r_w^2 + (r_w^2 - 1)^2}}. \tag{88}$$

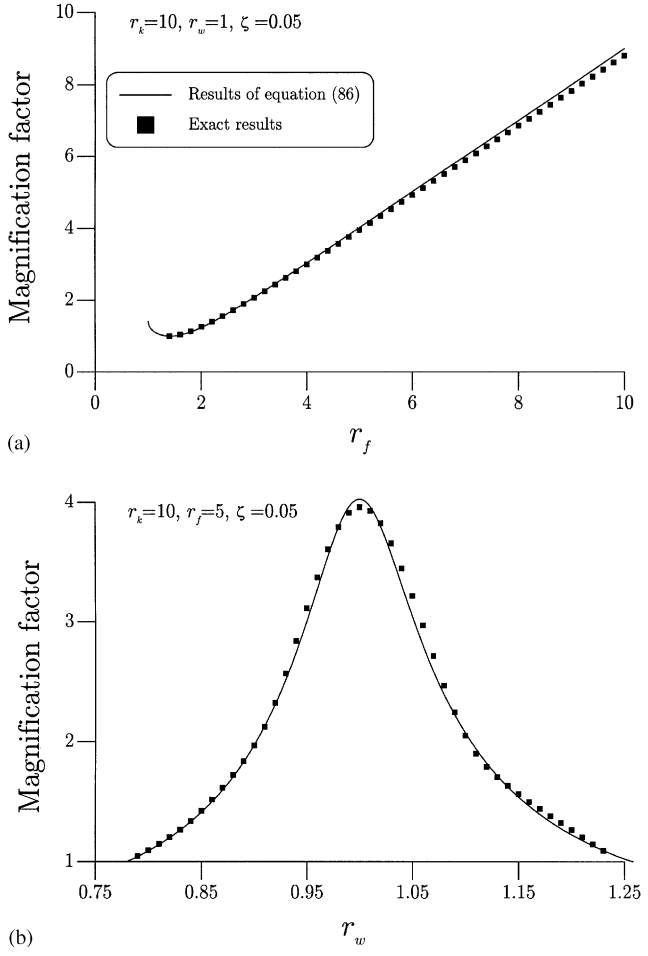

Fig. 7. Comparison of the magnification factor for the friction oscillator. The solid curves were calculated from formula (86) for different r_f's in (a) and different r_w's in (b). The results confirm the validity of formula (86).

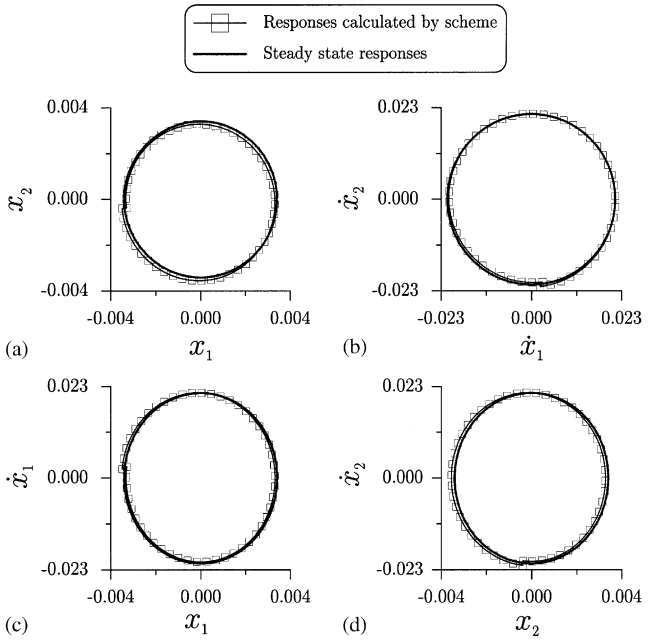

Fig. 8. Comparison of steady state responses in the phase planes (a) (x_1, x_2), (b) $(\dot{x}_1, \dot{x}_2)$, (c) $(x_1, \dot{x}_1)$, and (d) $(x_2, \dot{x}_2)$.

This formula tells us the minimum force ratio required (the minimum driving force amplitude required if the friction force bound is known and the maximum friction force bound allowed if the driving force amplitude is known) to avoid sticking in terms of the other parameters r_k, r_w and ζ.

In Fig. 7(a) the magnification factor as given by Eq. (86) is plotted with respect to r_f for fixed values of $r_w = 1$, $r_k = 10$, and $\zeta = 0.05$. In Fig. 7(b) the magnification factor is plotted with respect to r_w for fixed values of $r_f = 5$, $r_k = 10$, and $\zeta = 0.05$. Both the results are compared with the (highly accurate, almost exact) values numerically calculated by the group-preserving scheme, confirming that the handy formula (86) is capable of estimating the magnification factor. Having substituted Eq. (86) for $\hat{x}_0$ and Eq. (82) for ϕ in Eqs. (50) and (51), we plotted the steady state phase portraits in Fig. 8 under the following parameters: $r_f = 10$, $r_k = 1$, $r_w = 2$, and $\zeta = 0.02$. Comparing with the steady state responses during the 19th period calculated by the numerical scheme shows that the above handy estimations match the (almost exact) results very well. According to formula (86), we plotted the magnification factor with respect to r_w for different values of $\zeta = 0, 0.04, 0.08, 0.12, 0.16, 0.2$, and fixed values of $r_f = 10$ and $r_k = 2$ in Fig. 9(a), and also with respect to r_k for different values of $\zeta = 0, 0.04, 0.08, 0.12, 0.16, 0.2$, and fixed value of $r_w = 1.1$ in Fig. 9(b).

For the energy dissipation purposes we usually hope the oscillator can operate in the sliding phase permanently and without sticking, and thus consumes the input energy continuously. Eq. (88) provides a minimum requirement of the driving force amplitude p_0 (when r_y is already given) or a maximum bound of the friction force (when p_0 is already given) to render the friction oscillator vibratory in the steady state sliding phase. We plot the minimum curves for different values of $\zeta = 0, 0.04, 0.08, 0.12, 0.16, 0.2$, and fixed value of $r_k = 2$ in Fig. 10(a). The damping ratio

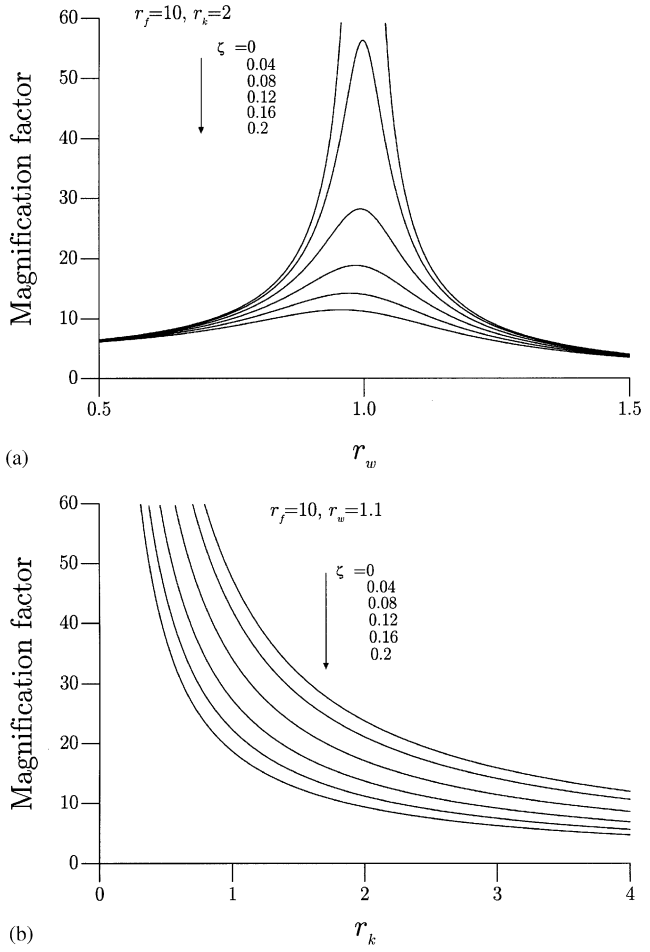

Fig. 9. (a) The $\hat{x}_0$ versus r_w curves with fixed $r_f = 10$, $r_k = 2$ and different ζ's, and (b) the $\hat{x}_0$ versus r_k curves with fixed $r_f = 10$, $r_w = 1.1$ and different ζ's, all calculated from Eq. (86).

has little influence on r_f in the range of lower and higher frequency ratios. If the applied load p_0 is large enough or in converse the friction force bound r_y is small enough, rendering the ratio $r_f = p_0/r_y$ over the values predicted by the minimum curves, the oscillator will settle down to the steady state sliding motion. Otherwise, the oscillator may respond consecutively in the two phases as shown in Fig. 5, and never comes to a steady state sliding phase. Sometimes we may want to know what r_f is required to obtain a certain value of the magnification factor $\hat{x}_0$. From Eqs. (75) and (76)–(78) it follows that

$$r_f = \sqrt{1 + 2r_k(1 - r_w^2) + r_k^2[4\zeta^2 r_w^2 + (r_w^2 - 1)^2]\hat{x}_0^2 + 4\zeta r_k r_w \sqrt{\hat{x}_0^2 - 1}}. \tag{89}$$

In Fig. 10(b) we plot the above r_f with respect to r_w for different values of $\hat{x}_0 = 1.5, 2.5, 3.5, 4.5, 5.5, 6.5$, and fixed values of $\zeta = 0.02$ and $r_k = 2$.

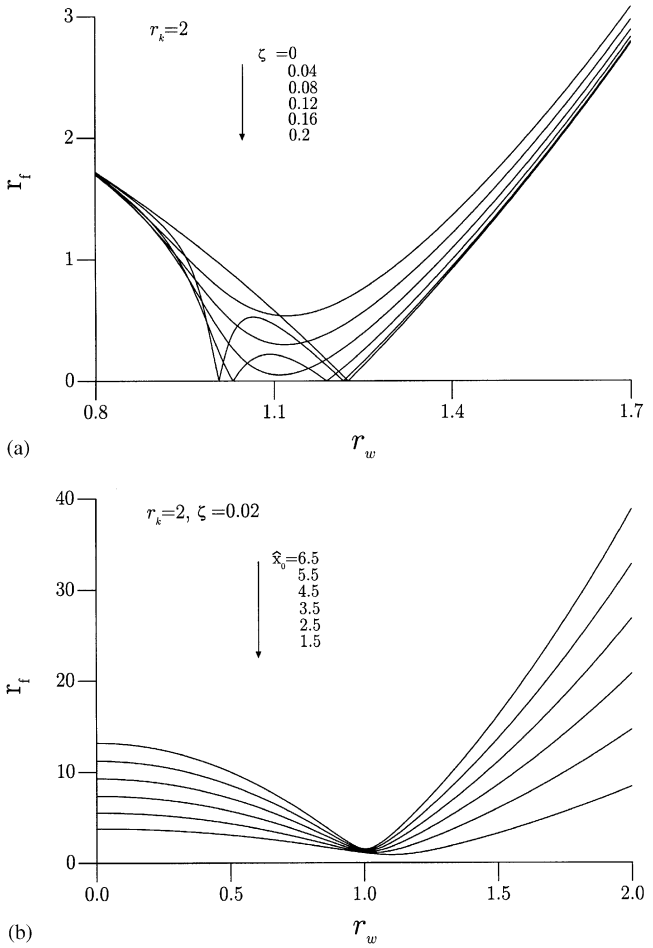

Fig. 10. (a) The minimum force ratio (88) required to render the friction oscillator in the steady state sliding motion for fixed $r_k = 2$ and different values of the damping ratio ζ, and (b) the force ratio required to achieve a certain values of the magnification factor $\hat{x}_0$ for fixed $r_k = 2$ and $\zeta = 0.02$.

8. Friction oscillator with rigid support

For the case of $k_d = \infty$ we obtain a two-dimensional friction oscillator with rigid support. Such model is usually adopted by engineers to analyze the support friction behaviour of structures or equipment directly sitting on the floor or ground or with support of the bulk type. Such model is indeed a limiting case of the model studied in Sections 2–7. Most results obtained above are still applicable, but some modifications need to be done as follows.

8.1. Numerical scheme

For the two-dimensional friction oscillator with planar rigid support the following numerical scheme can be derived:

$$x_1(n+1) = x_1(n) + \Delta t y_1(n), \tag{90}$$

$$x_2(n+1) = x_2(n) + \Delta t y_2(n), \tag{91}$$

$$y_1(n+1) = y_1(n) - \frac{\Delta t}{m}[kx_1(n) + cy_1(n) + r_1^a(n) - p_1(n) + c_1], \tag{92}$$

$$y_2(n+1) = y_2(n) - \frac{\Delta t}{m}[kx_2(n) + cy_2(n) + r_2^a(n) - p_2(n) + c_2], \tag{93}$$

$$r_1^a(n+1) = \frac{r_y y_1(n+1)}{\sqrt{y_1^2(n+1) + y_2^2(n+1)}}, \tag{94}$$

$$r_2^a(n+1) = \frac{r_y y_2(n+1)}{\sqrt{y_1^2(n+1) + y_2^2(n+1)}}. \tag{95}$$

Eqs. (94) and (95) are the direct results of Eq. (5) by substituting $\dot{\lambda} = \|\dot{\mathbf{x}}\|$, which follows from Eq. (10) by letting $\dot{\mathbf{x}}^f = \dot{\mathbf{x}}$, since $\dot{\mathbf{x}}^e = \mathbf{0}$ due to the rigid support. It is easy to see that $(r_1^a)^2(n+1) + (r_2^a)^2(n+1) = r_y^2$ in the sliding phase. The above last two equations are independent of the time step size. A typical response is displayed in Fig. 11 for illustration, where the parameters used were $m = 1000/(4\pi)^2$ kN s^2/m ($= 10^6/(9.81 \times 16\pi^2)$ kg), $c = 10/\pi$ kN s/m, $k = 1000$ kN/m, $r_y = 30$ kN, $p_0 = 60$ kN, and $\omega_d = 8\pi$ rad/s.

8.2. Steady state motion

The rigid model is assumed subject to the same periodic input as given by Eqs. (37) and (38). First, we note that the phase lag ψ is $\pi/2$ upon letting $k_d = \infty$ ($r_k = 0$) in Eq. (61), which indicates that the displacements and friction forces have a phase lag $\pi/2$. Second, dividing Eqs. (65) and (66) by p_0, and letting $\psi = \pi/2$ in these two equations we obtain

$$(r_w^2 - 1)\hat{x}_0 + \cos\phi = 0, \tag{96}$$

$$2\zeta r_w \hat{x}_0 - \frac{1}{r_f} - \sin\phi = 0, \tag{97}$$

where, instead of definition (69),

$$\hat{x}_0 := \frac{kx_0}{p_0} \tag{98}$$

is the magnification factor for the rigid model. Substituting Eq. (96) for $\cos\phi$ and Eq. (97) for $\sin\phi$ in the identity $\cos^2\phi + \sin^2\phi = 1$, we obtain a single equation for $\hat{x}_0$,

$$\hat{b}_2\hat{x}_0^2 - \hat{b}_3\hat{x}_0 - \hat{b}_1 = 0, \tag{99}$$

where

$$\hat{b}_1 := 1 - \frac{1}{r_f^2}, \tag{100}$$

$$\hat{b}_2 := 4\zeta^2 r_w^2 + (r_w^2 - 1)^2, \tag{101}$$

$$\hat{b}_3 := \frac{4\zeta r_w}{r_f}, \tag{102}$$

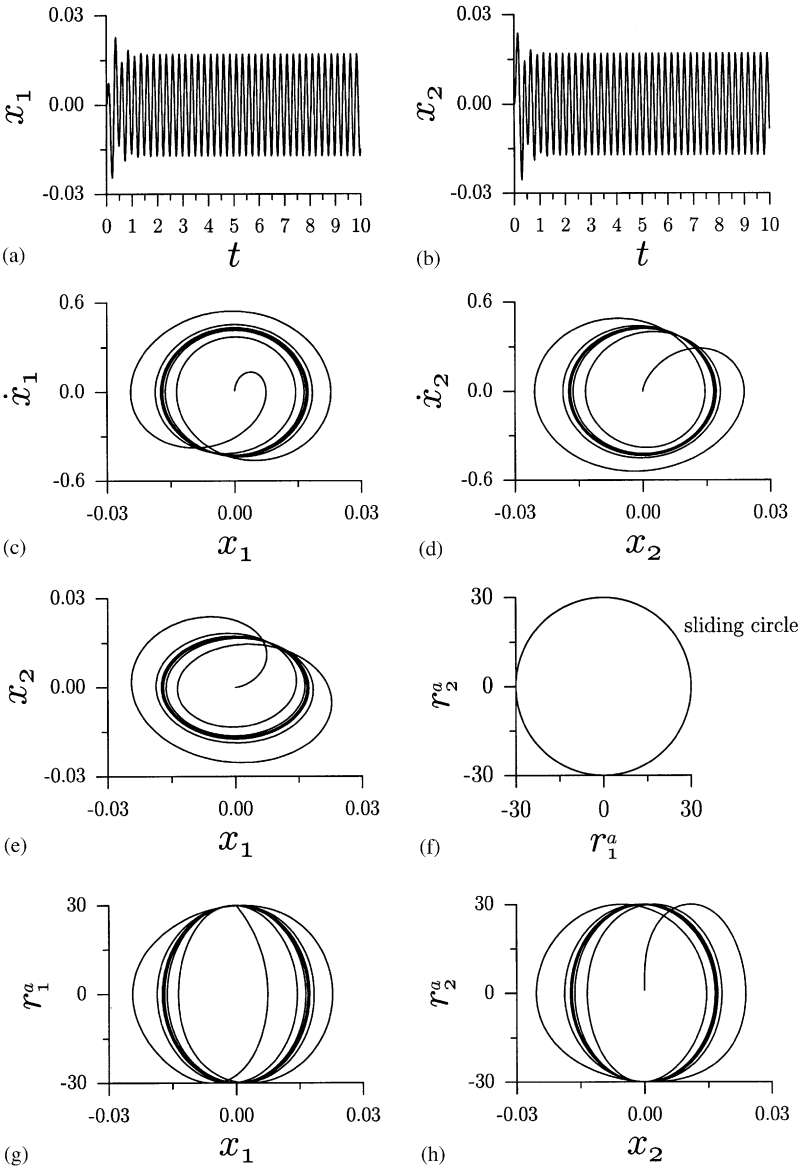

Fig. 11. A typical response of the two-dimensional friction oscillator under large driving force showing steady state behaviour. Time histories of displacements: (a) x_1 and (b) x_2, and of velocities (c) $\dot{x}_1$ and (d) $\dot{x}_2$; response paths of (x_1, x_2) in (e) and of (r_1^a, r_2^a) in (f); and dissipation loops of (x_1, r_1^a) in (g) and of (x_2, r_2^a) in (h).

in which r_f, r_w and ζ have been defined in Eqs. (70)–(73). Solving Eq. (99) for $\hat{x}_0$ we obtain

$$\hat{x}_0 = \frac{\hat{b}_3 + \sqrt{\hat{b}_3^2 + 4\hat{b}_1\hat{b}_2}}{2\hat{b}_2}. \tag{103}$$

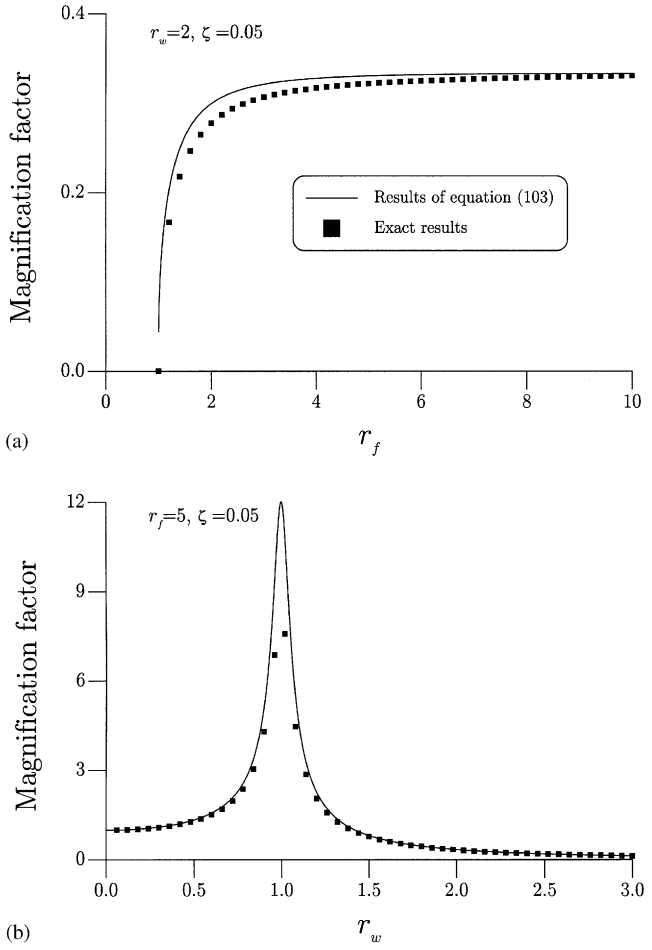

Fig. 12. Comparison of the magnification factor for the friction oscillator with rigid support. The solid curves were calculated from formula (103) for different r_f's in (a) and different r_w's in (b). The results confirm the validity of formula (103).

Due to $\hat{b}_2 > 0$, the above formula is well defined only for $r_f \geqslant 1$. The phase lag ϕ follows from Eqs. (96) and (97),

$$\phi = arctan \frac{2\zeta r_w \hat{x}_0 - 1/r_f}{(1 - r_w^2)\hat{x}_0}. \tag{104}$$

In Fig. 12(a) the magnification factor as given by Eq. (103) is plotted with respect to r_f for fixed values of $r_w = 2$ and $\zeta = 0.05$. In Fig. 12(b) the magnification factor is plotted with respect to r_w for fixed values of $r_f = 5$ and $\zeta = 0.05$. Both results are compared with the (highly accurate, almost exact) values numerically calculated by the group-preserving scheme, confirming that the handy formula (103) is very good to estimate the magnification factor.

For the no-viscous-damping case, i.e., $\zeta = 0$, we have

$$\hat{x}_0 = \sqrt{\frac{1}{(r_w^2 - 1)^2} - \frac{1}{r_f^2 (r_w^2 - 1)^2}}. \tag{105}$$

The corresponding formula of the maximum displacement for the one-dimensional Coulomb friction oscillator subjected to harmonic excitation $p_0 \sin \omega_d t$ has been derived in Ref. [21],

$$\hat{x}_0 = \sqrt{\frac{1}{(1 - r_w^2)^2} - \frac{1}{r_f^2 r_w^2} \left(\frac{\sin(\pi / r_w)}{1 + \cos(\pi / r_w)} \right)^2}. \tag{106}$$

In Fig. 13 the variations of the above two $\hat{x}_0$'s with respect to r_w are compared. The two oscillators, although with different dimensions, give almost the same magnification factors for most frequency ratios.

Substituting Eqs. (100)–(102) into the equality $4\hat{b}_1 \hat{b}_2 + \hat{b}_3^2 = 0$ we obtain

$$r_f = \sqrt{\frac{(r_w^2 - 1)^2}{4\zeta^2 r_w^2 + (r_w^2 - 1)^2}}. \tag{107}$$

This equation gives a closed-form formula of the border surface in the parametric space (r_f, r_w, ζ) for the steady state sliding oscillations of the two-dimensional friction oscillator with rigid support. It provides engineers the minimum driving force amplitude required to avoid sticking for different friction force bounds and different frequency ratios. In Fig. 14 it is displayed as the solid

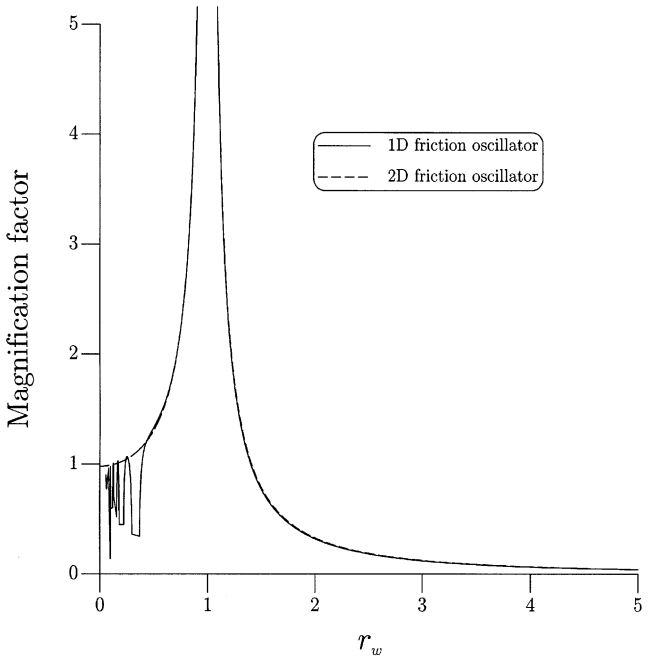

Fig. 13. The magnification factor versus the frequency ratio r_w for the one- and two-dimensional friction oscillators.

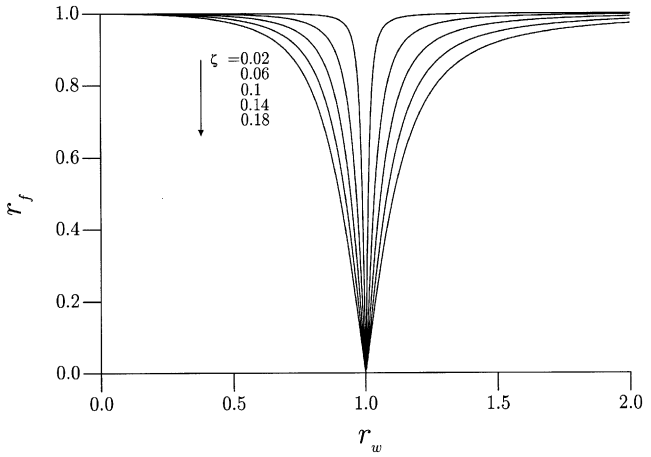

Fig. 14. The minimum force ratio required to avoid sticking. The curves represent Eq. (107) for different values of the damping ratio ζ.

lines for different values of $\zeta = 0.02, 0.06, 0.1, 0.14, 0.18$. The r_f which is greater than what the above formula predicts will make the oscillator oscillate without sticking in the steady state. For lower and higher frequency ratios the damping ratio gave little influence on r_f as shown in Fig. 14.

9. Conclusions

We have shown that a two-dimensional friction oscillator can be described completely by model (1)–(9). This oscillator can be applied to study the hysteretic behaviour of building base isolation and also vibration abatement of turbomachinery blades. Both have widespread applications. Precise criteria for sliding and sticking of the oscillator were derived. We developed a group-preserving scheme to calculate the responses, which could update the friction force to fulfill the sliding conditions without any iteration at all and, thus, provided very well computational accuracy and efficiency. For harmonic excitations several examples were given to show the behaviour of various responses. The simple harmonic balance method was employed to estimate the steady state responses. The closed-form formula of the magnification factor was derived in terms of the four dimensionless ratios instead of the original seven system parameters. The formula supplied handily very good estimations when compared with the numerical results calculated by the group-preserving scheme. The closed-form formula (88) of the border surface in the parametric space for non-sticking and sticking oscillations was now available. When the stiffness of the damper plate tends to infinity, we have a two-dimensional friction oscillator with rigid support, for which formulae (103) and (107) were derived to calculate the magnification factor and the minimum force ratio for the sliding oscillations, respectively. In view of the detrimental effect of sticking on the operation and performance of oscillators (e.g., machine parts), these handy formulae must be very useful for engineers to select a minimum driving force

amplitude or a maximum friction force bound to prevent an oscillating object from sticking to the friction surface.

References

[1] B. Feeny, A. Guran, N. Hinrichs, K. Popp, A historical review on dry friction and stick-slip phenomena, Applied Mechanics Review 51 (1998) 321–341.
[2] R.A. Ibrahim, Friction-induced vibration, chatter, squeal, and chaos, Part I: mechanics of contact and friction, Part II: dynamics and modeling, Applied Mechanics Reviews 47 (1994) 209–253.
[3] R.I. Skinner, W.H. Robinson, G.H. Mcverry, An Introduction to Seismic Isolation, Wiley, New York, 1993.
[4] J.H. Griffin, Friction damping of resonant stresses in gas turbine engine airfoils, Journal of Engineering for Power, American Society of Mechanical Engineers 102 (1980) 329–333.
[5] A.V. Srinivasan, D.G. Cutts, Measurement of relative vibratory motion at the shroud interfaces of a fan, Journal of Vibration, Acoustics, Stress, and Reliability in Design, American Society of Mechanical Engineers 106 (1984) 189–197.
[6] A. Zmitrowicz, A vibration analysis of a turbine blade system damped by dry friction forces, International Journal of Mechanical Science 23 (1981) 741–746.
[7] F. Pfeiffer, On stick–slip vibrations in machine dynamics, Ingenieria Archiv 54 (1992) 232–240.
[8] P. Popp, P. Stelter, Nonlinear oscillations of structures induced by dry friction, in: W. Schiehlen (Ed.), IUTAM Symposium on Nonlinear Dynamics in Engineering Systems, Springer, Berlin, 1990, pp. 233–240.
[9] W.W. Tworzydlo, E.B. Becker, J.T. Oden, Numerical modeling of friction-induced vibrations and dynamic instabilities, Applied Mechanics Reviews 47 (1994) 255–274.
[10] H.-K. Hong, C.-S. Liu, Coulomb friction oscillator: modelling and responses to harmonic loads and base excitations, Journal of Sound and Vibration 229 (2000) 1171–1192.
[11] J.H. Griffin, C.-H. Menq, Friction damping of circular motion and its implications to vibration control, Journal of Vibration and Acoustics, American Society of Mechanical Engineering 113 (1991) 225–229.
[12] C.-H. Menq, P. Chidamparam, J.H. Griffin, Friction damping of two-dimensional motion and its application in vibration control, Journal of Sound and Vibration 144 (1991) 427–447.
[13] C.-H. Menq, B.D. Yang, Non-linear spring resistance and friction damping of frictional constraint having two-dimensional motion, Journal of Sound and Vibration 217 (1998) 127–143.
[14] K.Y. Sanliturk, D. Ewins, Modelling two-dimensional friction contact and its application using harmonic balance method, Journal of Sound and Vibration 193 (1996) 511–523.
[15] W. Sextro, K. Popp, I. Wolter, Improved reliability of bladed disks due to friction dampers, ASME Paper 97-GT-189, 1997.
[16] C.-S. Liu, Two-dimensional bilinear oscillator: group-preserving scheme and steady state motion under harmonic loading, International Journal of Non-Linear Mechanics (2003), to appear.
[17] B.D. Yang, C.-H. Menq, Characterization of contact kinematics and application to the design of wedge dampers in turbomachinery blading, Part I: stick–slip contact kinematics, ASME Paper 97-GT-19, 1997.
[18] B.D. Yang, M. Chu, C.-H. Menq, Stick-slip-separation analysis and non-linear stiffness and damping characterization of friction contacts having variable normal load, Journal of Sound and Vibration 210 (1998) 461–481.
[19] J.L. Almazán, J.C. dela Llera, J.A. Inaudi, Modelling aspects of structures isolated with the frictional pendulum system, Earthquake Engineering and Structural Dynamics 27 (1998) 845–867.
[20] C.-S. Liu, Cone of non-linear dynamical system and group preserving schemes, International Journal of Non-Linear Mechanics 36 (2001) 1047–1068.
[21] H.-K. Hong, C.-S. Liu, Non-sticking oscillation formulae for Coulomb friction under harmonic loading, Journal of Sound and Vibration 244 (2001) 883–898.